ЕЛЕКТРИЧНА КОЛА, ЕЛЕКТРИЧНИ СИСТЕМИ И ОБРАДА СИГНАЛА
/
ELECTRIC CIRCUITS AND SYSTEMS, AND SIGNAL PROCESSING

(ЕК/EKI)

Kristalni filtri za opseg frekvencija 150-170MHz

Dragi Dujković, Irini Reljin, Lenkica Grubišić, Snežana Dedić-Nešić, Ana Gavrovska

Apstrakt—**Tehnologija izrade filtara zasnovanih na kristalima kvarca je i dalje zahtevan tehnološki postupak iako je imao svoj maksimum osamdesetih godina prošlog veka. Međutim, i danas se koriste ove komponente u savremenim telekomunikacijama, naročito digitalnim, i to tamo gde je veoma bitno imati kvalitetne uređaje za prijem, predaju i prenos signala. Uslovi rada filtara i uređaja u koji su ugrađeni, pored električnih zahtevaju i dobre klimomehaničke radne karakteristike koje su definisane zahtevima korisnika. U radu su opisani kristalni filtri propusnici opsega, namenjeni za rad u spoljnim uslovima pri visokim frekvencijama, i to u opsegu od 150 do 170 MHz.**

***Ključne reči*—Kristali, filtriranje, projektovanje, kućište, tehničke karakteristike.**

I. UVOD

Kristalni filtri koji se implementiraju u uređaje za razne civilne i vojne namene, često imaju strogo definisane zahteve vezane za električne karakteristike, ali i za takozvane klimomehaničke karakteristike pri kojima su iskazani uslovi funkcionisanja filtra pri specifičnim uslovima namene (ovo je uobičajeno za uređaje koji se koriste van zaštite prostorija, tj. u spoljnim i terenskim uslovima rada).

U radu je opisan razvoj novih tipova kristalnih filtara propusnika opsega učestanosti na frekvencijama od 150 do 170MHz prema specifikacijama definisanim od strane korisnika. Specifikacija filtra obuhvata električne karakteristike koje definišu tok amplitudske karakteristike i klimomehaničke karakteristike koje definišu zahteve u pogledu vibracija, udara i temperature za rad filtra u specifičnim uslovima.

Razmatrani su izazovi ostvarivanja što većeg slabljenja u nepropusnom opsegu filtra i što manjeg slabljenja u propusnom opsegu filtra. Paralelno sa rešavanjem ovih problema odvijao se razvoj kristalnih jedinki u cilju ostvarivanja svih parametara koje je projekat filtra odredio a posebno ostvarivanja njihovog što većeg Q-faktora i što većeg faktora potiskivanja neželjenih rezonancija.

Takođe je urađena i analiza svih elemenata koji se u filtar ugrađuju i ispitan njihov uticaj na osetljivost filtra u pogledu funkcionisanja u radnom temperaturnom opsegu i pri ekstremnim zadatim uslovima rada [1-4].

Rad je organizovan na sledeći način. U drugoj glavi dat je kratak osvrt na potrebe za realizacijom ovakvih filtara. Treća glava je posvećena projektovanju filtara. Kristalne jedinke su opisane, kao i sama realizacija u glavi četiri. U petom poglavlju se nalazi zaključak.

II. POTREBA ZA REALIZACIJOM FILTARA KONKRETNIH KARAKTERISTIKA

Zahtevane električne karakteristike filtara su direktno vezane za namenu uređaja, a ta namena određuje tok amplitudske i fazne karakteristike u propusnom opsegu, centralnu frekvenciju filtra, širinu propusnog opsega i selektivnost.

U zavisnosti od toga u kakvim će uslovima uređaj funkcionisati zahtev za specifikaciju pored standardnih električnih karakterisrtika ima i zahteve koji se odnose na vibracije, udare, potrese, temperaturu, pritisak, vlagu (tzv. klimomehaničke uslove rada) ali i mnoge druge specifične zahteve.

Ovakvi kristalni filtri za specijalne namene, koji se prema zadatoj specifikaciji ne mogu pronaći u katalozima proizvođača, zahtevaju razvoj uz odgovarajući projekat filtra prema postavljenim zahtevima.

U celom svetu postoji samo nekoliko proizvođača koji mogu realizovati kristalne filtre na osnovu specifičnih zahteva korisnika. To zahteva razvoj novih tehnoloških postupaka pri proizvodnji, kao i projektovanje filtara i njihovih komponenata. Zbog toga se većina proizvođača bavi proizvodnjom kataloških tipova filtara sa standardnim karakteristikama i komponentama [4–10].

III. PROJEKTOVANJE FILTARA

Urađen je projekat filtra čija je lista tehničkih zahteva data u tabeli1. Na osnovu definisanih zahteva u pogledu toka amplitudske karakteristike u propusnom i nepropusnom opsegu određen je red filtra i mreža koja obezbeđuje ispunjavanje postavljenih zahteva (videti sliku 1). Pri proračunu filtra se mora voditi računa o tolerancijama elemenata koji se ugrađuju u filtar, da bi on mogao ispuniti tražene karakteristike.

Prema predviđenim gubicima u mreži, urađen je proračun filtra, određena električna šema i definisani zahtevi vezani za kristalne jedinke. Projektom filtra su tačno definisani svi zahtevi koji se odnose na parametre kristalnih jedinki, njihove vrednosti i tolerancije. Definisani su i zahtevi u pogledu frekvencija kristala, serijske i paralelne kapacitivnosti kristala i podešenosti frekvencije na sobnoj temperaturi. Takođe su definisane i maksimalna dozvoljena odstupanja frekvencija kristala u radnom temperaturnom

Dragi Dujković – Elektrotehnički fakultet, Univerzitet u Beogradu, Bulevar Kralja Aleksandra 73, 11020 Beograd, Srbija (e-mail: dragi@etf.bg.ac.rs).
Irini Reljin – Elektrotehnički fakultet, Univerzitet u Beogradu, Bulevar Kralja Aleksandra 73, 11020 Beograd, Srbija (e-mail: dragi@etf.bg.ac.rs).
Lenkica Grubišić – Institut Mihajlo Pupin, Volgina 15, 11060 Beograd, Srbija (e-mail: lenka@piezo.imp.bg.ac.rs).
Snežana Dedić-Nešić– Institut Mihajlo Pupin, Volgina 15, 11060 Beograd, Srbija (e-mail: snezanadn@gmail.com).
Ana Gavrovska – Elektrotehnički fakultet, Univerzitet u Beogradu, Bulevar Kralja Aleksandra 73, 11020 Beograd, Srbija (e-mail: dragi@etf.bg.ac.rs).

opsegu filtra. Na osnovu zahteva za ispunjavanje klimomehaničkih uslova rada odabran je i tip kućišta kristalnih jedinki.

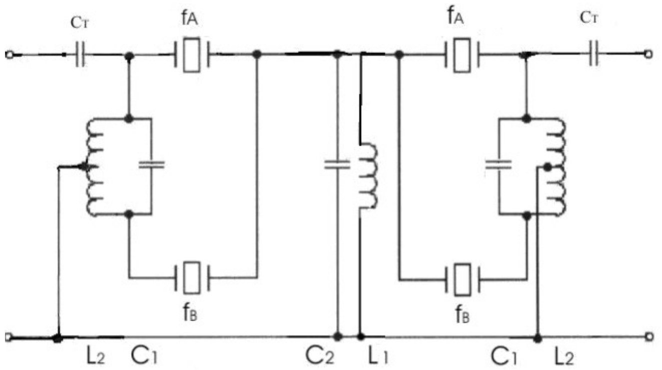

Sl. 1. Električna šema kristalnog filtra 156.800 MHz.

Prema definisanim zahtevima sadržanim u specifikaciji filtra (Tabela I) urađen je projekat filtra 4-og reda uz Chebyshev aproksimaciju. Razvijene su mikrominijaturne kristalne jedinke AT-reza sa malim odstupanjem frekvencije u širokom temperaturnom opsegu koje ispunjavaju postavljene zahteve u pogledu položaja i potisnutosti sporednih rezonancija i u pogledu zahtevanih klimo-mehaničkih karakteristika.

Proračunom filtra osim kristalnih jedinki određuju se i vrednosti ostalih komponenata, kao što su kalemovi i kondenzatori kao i njihov raspored na štampanoj ploči.

Treba imati u vidu da filtri rade na visokim frekvencijama gde prisustvo parazitnih kapacitivnosti značajno utiče na karakteristike filtara, tako da je raspored komponenata od izuzetnog značaja u rešavanju problema selektivnosti i slabljenja u nepropusnom opsegu filtra [1-5].

Da bi izmerili amplitudne i fazne karakteristike, za merenja je korišćen realizovani kristalni filtar centralne frekvencije 156.800 MHz. Ovaj filtar ima relativno slabljenje u propusnom opsegu +/- 7.5 kHz manje od 3dB. Izvan frekventnog opsega +/-60 kHz slabljenje je veće od 40 dB . U širem opsegu frekvencija, do +/- 50 MHz, relativno slabljenje je veće od 40 dB.

Minimalno pogonsko slabljenje filtra je manje od 6 dB. Talasnost u propusnom opsegu je manja od 1 dB. Ulazna i izlazna otpornost filtra iznose 50 Ω.

Radni temperaturni opseg filtra je -20º C do +70 ºC. Temperaturni opseg skladištenja (opseg temperatura u kojima filtar neće promeniti karakteristike dok se čuva u skladištu) je -40 ºC do +85 ºC. Filtar je smešten u kućište dimenzija (61×26.2×26.2) mm.

Filtar takođe mora da ispuni posebne zahteve vezane za vibracije, udare i temperaturu, tj. da zadovolji zahteve za klimomehaničke karakteristike rada. Detalji svih tehničkih karakteristika filtra su dati u Tabeli I.

IV. Pristup zasnovan na kristalnim jedinkama i realizovani kristalni filtar

Kristalne jedinke (KJ) su planparalelne, prečnika Φ=5 mm. Upotrebljena je elektroda d=0.79mm. Planparalelne KJ su sečene u obliku kruga tako da su im bočne strane paralelne [10]. Kao elektrodni materijal korišćen je aluminijum. U proizvodnji se mora voditi računa o planparalelnosti radi ostvarenja zahteva vezanih za položaj i potisnutost sporednih rezonancija.

Za nosač kristalne jedinke upotrebljen je držač sa petljicama da bi se obezbedili najpovoljniji rezultati vezani za zahteve na otpornost rada kristalne jedinke pri uticaju vibracija i mehaničkih udara.

Na slici 2 prikazan je realizovani filtar. Filtar je smešten u standardno G10BNC kućište koje je prikazano na slici 3.

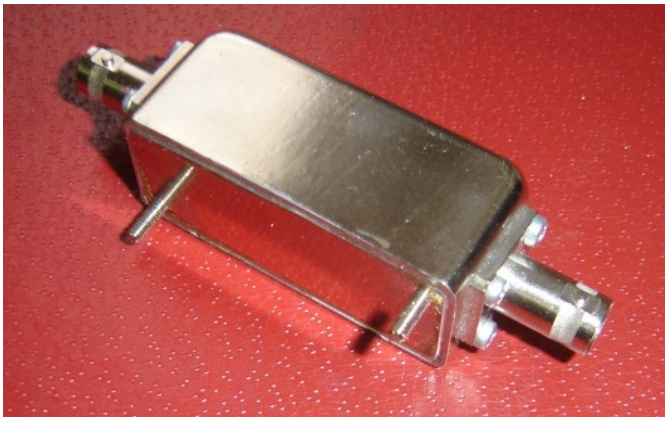

Sl. 2. Realizovani kristalni filtar.

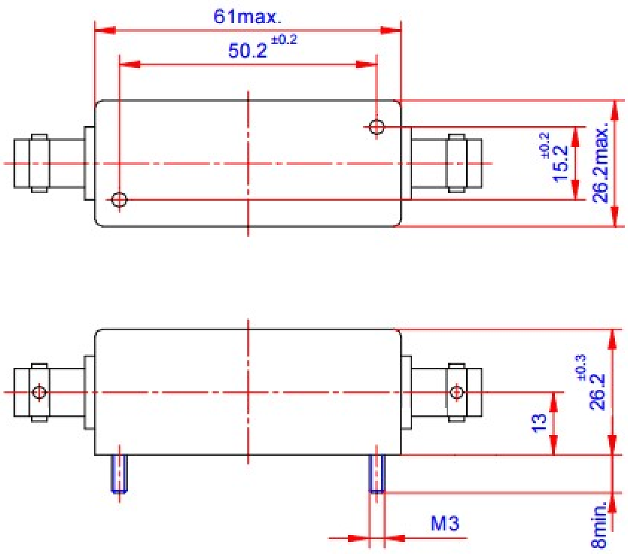

Sl. 3. Kućište G10 BNC.

Rezultati ispitivanja filtara na sobnoj temperaturi i u radnom temperaturnom opsegu od -40°C do +85°C pokazuju da filtri ispunjavaju zahteve navedene u listi tehničkih podataka.

Rezultati merenja amplitudske karakteristike filtra na sobnoj temperaturi prikazani su u dijagramima na slici 4.

Na filtrima je sprovedeno merenje električnih karakteristika i testiranje prema zadatim uslovima. Konačni rezultati merenja pokazali su da su karakteristike realizovanih filtara u skladu sa zahtevima definisanim listom tehničkih podataka i da primenjeni tehnološki postupak daje visokokvalitetan filtar koji se može koristiti i u posebnim klimatskim i mehaničkim uslovima [4-8].

Lista tehničkih podataka za kristalne filtre 150-170 MHz je sledeća:

1. Kućište CW-HC-45
2. Q-faktor > 60000
3. dinamička kapacitivnost $C_1 = 0.85$ mpF ± 10%
4. paralelna kapacitivnost $C_o = 0.6$ pF ± 5%
5. dinamička otpornost $R_1 < 220\ \Omega$
6. podešenost df/f=±5 ppm
7. odstupanje df/f=±20 ppm
8. starenje df/f=1 ppm/god
9. radni temperaturni opseg -20÷+70˚C
10. neželjene rezonancije A. f_0+50 kHz–bez f_n
    B. f_n>30 dB za f_0±1 MHz

Tabela I Tehničke karakteristike filtara

Centralna frekvencija(CF)	150 - 170 MHz
Širina propusnog opsega na 3 dB	+/- 7.5 kHz
Talasnost u propusnom opsegu	1 dB max u opsegu +/- 7.5 kHz
Širina nepropusnog opsega na 40 dB	+/- 60 kHz max
Relativno slabljenje u nepropusnom opsegu	40 dB min za +/- 50 MHz
Minimalno pogonsko slabljenje	6 dB max
Ulazna impedansa	50 Ω
Izlazna impedansa	50 Ω
Dozvoljeni nivo neželjenih rezonancija	10 dB min
Radni temperaturni opseg	-20 ºC до +70 ºC
Temperaturni opseg skladištenja	-40 ºC до +85 ºC
Vibracije sinusne	10 do 2000 Hz 30 g
Udari	100 g 6 ms
Termički šok 5 ciklusa	-55 ºC do +125 ºC

V. Zaključak

Pored proračuna i realizacije kristalnog filtra, razvijena je i nova kristalna jedinka. Ovakvi kristalni filtri predstavljaju novi proizvod, jer su u njemu korišćene nove tehnologije i nove komponente. Ovi proizvodi imaju širok dijapazon primena i veliku upotrebnu vrednost i ističu se svojom cenom i svojim kvalitetom, tako da su konkurentni ne samo na domaćem tržištu već i u celom svetu. Navedene karakteristike i konkurentnost na svetskom tržištu daju perspektivu razvoju novih elektronskih sklopova i proizvoda na bazi kristalne jedinke.

U daljem razvoju ovih i sličnih uređaja treba ići na usvajanje novih tehnologija izrade kristalnih jedinki i upotrebe novih i kvalitetnijih komponenti u kolu elektronskih sklopova novih uređaja [4-8].

Zahvalnica

Istraživanja opisana u ovom radu su delimično finansirana od strane Ministarstva za obrazovanje i nauku Republike Srbije.

Literatura

[1] Snežana Dedić-Nešić “Prilog projektovanju kristalnih filtara sa linearnom faznom karakteristikom” Magistarska teza, Elektrotehnički fakultet Beograd, 1991.

[2] A.I.Zverev: “Handbook of Filter Synthesis” John Wiley and Sons, Inc, 1967

[3] H. J. Blinchikoff, A. I. Zverev “Filtering in the Time and Frequency Domains” John Wiley and Sons, Inc, 1976

[4] D. S. Humpherys “The Analysis, Design and Synthesis of Electrical Filters” Prentice Hall, Englewood Clifs, N.J. 1970

[5] Snežana Dedić-Nešić, Dragi Dujković, Lenkica Grubišić, Irini Reljin, Branimir Reljin “Novi visokokvalitetni 90.1105 MHz filtri za komunikacije u rudnicima” ETRAN, 2010

[6] Dragi Dujković, Branimir Reljin, Snežana Dedić-Nešić, Lenkica Grubišić, Dubravka Jevtić , “Novi kristalnih filtar F121” ETRAN, 2012

[7] D. M. Dujković, S. Dedić–Nešić , L. Grubišić, A. Gavrovska, and I. Reljin, “High-quality crystal filter: Design and realization,” Telfor J., vol. 5, no. 2, pp. 118–122, 2013.

[8] D. M. Dujković, S. Dedić–Nešić, L. Grubišić, M. Paskaš, and I.Reljin, “Matched Crystal Filters” Telfor Proceedings, pp. pp. 481-484, Belgrade 2014.

[9] D. M. Dujković, S. Dedić–Nešić, L. Grubišić, M. Paskaš, and I. Reljin, “A Novel 76.8375 MHz Crystal Filter Based on Third Overtone Crystal Units“, Telfor Proceedings, pp. 177-181, Belgrade 2020.

[10] L. Grubišić, S. Dedić–Nešić, D. M. Dujković, , B. Reljin, “Novi tip kristalne jedinke za filtre namenjene za rad u posebnim klimo mehaničkim uslovima “, ETRAN, 2012, EK2.6-1-4, Banja Vrućica 2011.

Abstract

The technology of making filters based on quartz crystals is still a demanding technological process, although it had reached its maximum in the 1980s. However, even today, these components are used in modern telecommunications, especially digital, where it is very important to have high quality devices for receiving, transmitting and signal distribution. The operating conditions of the filters and devices in which they are installed, in addition to electrical ones, require good temperature-mechanical operating characteristics that are defined by the requirements made by users. The paper describes band-pass crystal filters, which are intended for operating in outdoor conditions at high frequencies in the range from 150 to 170MHz.

Crystal filters for frequency range 150-170 MHz

Dragi Dujkovic, Irini Reljin, Lenkica Grubisic, Snezana Dedic-Nesic, Ana Gavrovska

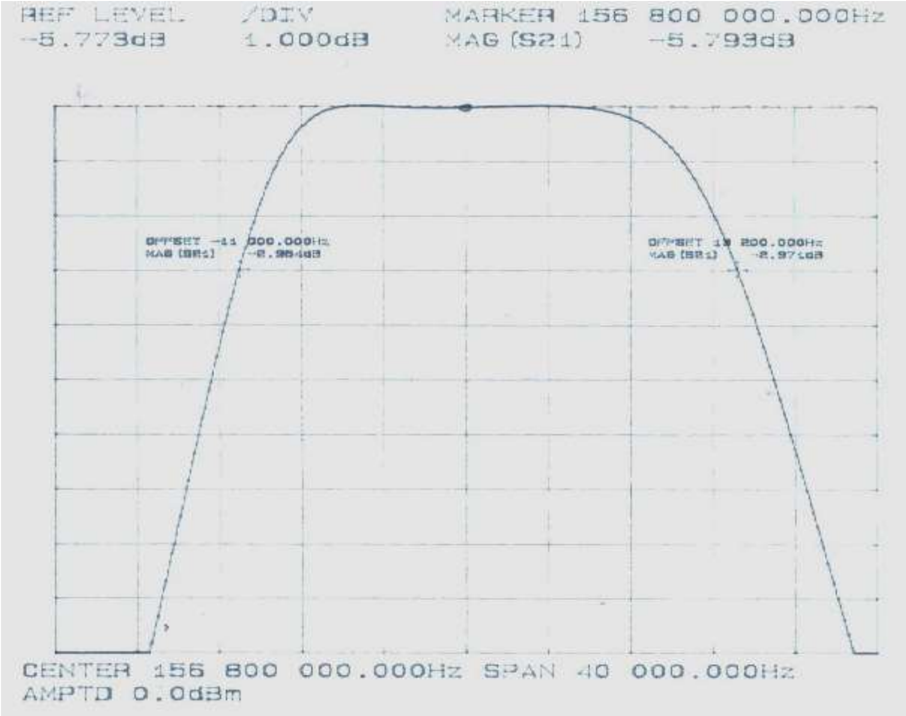

a)

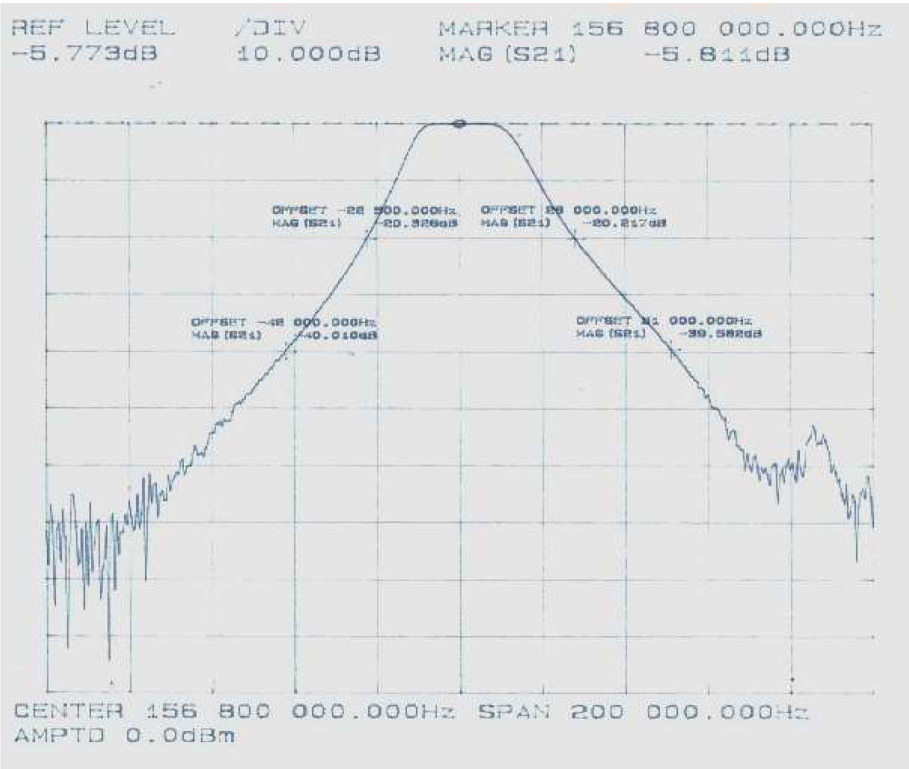

b)

Sl. 4. Rezultati merenja amplitudske karakteristike filtra 156.800 MHz na sobnoj temperaturi, a) u okviru radnog opsega +/- 7.5 kHz od CF , b) u okviru opsega od +/- 50 MHz od CF

Covid-19 and other CT Scan Authentication using Wavelet based Watermarking

Amra Gicić, and Ana Gavrovska, *Member, IEEE*

***Abstract*— Nowadays, it is essential to ensure the integrity of the medical image, especially for adequate region of interest (ROI) before taking any diagnostic decision, where watermarking is often used. In this paper, Covid-19 and other CT (Computerized Tomography) scans are analyzed using wavelet based watermarking under JPEG (Joint Picture Experts Group) compression attack. The structured method consisted of robust and fragile watermark, having in mind ROI, is implemented. JPEG compression attack is chosen since it is often used while saving case studies. This is of particular importance in the case of widely available Covid-19 CT scans of different resolutions. The CT scan structured watermarking shows promising results under JPEG attack. The results seem promising in both detection of image manipulation through fragile watermark and integrating visual logos through more robust approach.**

***Index Terms*— Medical images, Computerized Tomography, watermarking, wavelet, JPEG, DICOM, ROI.**

I. Introduction

Security risks of medical images can vary from unauthorized access to errors occurring during transmission in hospital information systems (HIS) and PACS (Picture archiving and communication system) [1-4]. An attached file or a packet header (as in DICOM (Digital Imaging and Communications in Medicine) files) often carries all information needed to identify a particular image. However, keeping image metadata in a separate header file is prone to forgeries or clumsy practices. An alternative would be to embed all such information into the image content itself.

Medical data security has become inevitable in smart hospital applications to ensure data privacy and patient data security of Electronic Patient/Health Records (EPR/EHR) [5-7]. Medical reports and images are transferred to physicians at distant locations and to other hospitals for diagnosis. Before making any diagnostic decision, the integrity of region of interest (ROI) of the received medical image must be verified. Watermarking can be used to ensure integrity and authentication of the medical image. Main challenges associated with e-healthcare systems and digital watermarking are following:

Amra Gicić is with the School of Electrical Engineering, University of Belgrade, Bulevar kralja Aleksandra 73, 11020 Belgrade, Serbia (e-mail: amragicic1625@gmail.com).

Ana Gavrovska is with the School of Electrical Engineering, University of Belgrade, Bulevar kralja Aleksandra 73, 11020 Belgrade, Serbia (e-mails: anaga777@gmail.com; anaga777@etf.rs).

- medical image and EPR transmission should not cause separation between metadata and image content,
- data (visual and non-visual) should not be modified accidentally or intentionally while transmitting over the insecure medium,
- medical information authentication should be ensured to obtain confirmation of content that belongs to the appropriate patient (origin and integrity authentication).

In this paper analysis is performed based on a structured watermarking method in order to protect medical images (modalities). The quality of the medical image, such as CT (computed/computerized tomography) scan, is considered for further use having in mind common JPEG (Joint Picture Experts Group) compression attack. Furthermore, a comparison is made with another structured watermarking method to verify the benefit of the implemented model.

The paper is organized as follows. After the introduction, in Section II ROI and RONI (region of non-interest) based watermarking is explained, as well as common techniques used for medical image watermarking. Implementation and extraction of the proposed structured RONI based watermark are briefly given in Section III. Experimental results are presented in Section IV. Conclusion is given in Section V.

II. ROI and RONI based watermarking for Medical images

A. *Medical image watermarking*

There are a lot of different watermarking methods, where wavelet and LSB (Least Significant Bit) based approaches are one of the most common [8-16]. Coatrieux et al. [8] proposed Region of Interest (ROI) based approach to preserve the diagnostically relevant region, and Region of Non-Interest (RONI) usage in order to keep integrity and to serve as watermark carrier. Mehta et al. [9] studied the performance of three different techniques in watermarking: DWT (Discrete Wavelet Transform), SVD (Singular Value Decomposition) and hybrid (DWT-SVD) based watermarking. Similarly, Navas et al. [10] proposed a method of non-blind transform domain watermarking using DWT-DCT-SVD approach (DCT- Discrete Cosines Transform). Fragile watermarking methods can be focused on ROI integrity, where approaches can also be block-based (Liew et al. [11], Tjokorda Agung [12]). Also, watermarking methods are designed for various modalities (e.g. Nambakhsh et al. [13] for protecting positron emission tomography - PET images, Castiglione et al. [14] for functional magnetic resonance imaging - fMRI images). Giakoumaki et al. [15] discussed the watermarking perspectives in a range of medical data management and distribution. The most common metadata structure correspond to DICOM standard, where the data is saved in the image header as a part of the image file and includes information related to patient, hospital, image, acquisition properties [16].

Different algorithms are available for ROI segmentation, and this depends on the medical image type. A physician can choose ROI in an image, where ROI represents rectangular area. In Fig.1 an example of segmentation of the ROI part for a CT image using a rectangular selection (rectangle) is illustrated.

Fig. 1. ROI segmentation for a CT image.

Moreover, there are various watermarks available. In Fig.2 visual and textual watermarks are illustrated: potential logo (logotype) representing clinics and text (txt) file representing information about the patient (PatientInfo), information about the image (ImageInfo), data about the diagnosis (DiagnosisInfo), data about the physician (PhysicianInfo). Such and additional data can also be found in the headers of DICOM format.

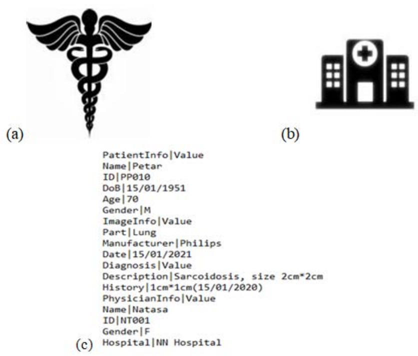

Fig. 2. Examples of visual watermarks (logos): (a) Logo1, (b) Logo2, and (c) a textual watermark.

B. *Robust and Fragile medical image authentication*

Watermarking often tends to be invisible and robust. On the other hand, some watermarks can be considered fragile if their usage is needed for detection of content manipulation. Thus, watermark can be considered as multiple or structured, having both robust and fragile part. If content manipulation occurs, fragile approach should prevent fragile watermark extraction. Fragile watermark can be of textual type, representing metadata. Also, robust watermark like logo can be invisible.

DWT enables energy compact representation of an image [9-10]. Using 1-level DWT decomposition image is transformed into four sub-bands: low-high (LH(1)), high-low (HL(1)), high-high (HH(1)) and low-low (LL(1)) band. LL band represents low frequency, HL and LH represent middle frequency (HL - horizontal and LH - vertical details) and HH represents high frequency band (diagonal image details), respectively. In 2-level DWT decomposition LL from the first level (noted as LL1) is further decomposed to additional four bands (LL2, LH2, HL2, HH2). The bands represented by wavelet coefficients can be used for embedding fragile and robust watermarks.

Direct embedding on the wavelet coefficients is not necessary. The embedding can be performed on the elements of singular values of the DWT sub-bands. This is done by SVD, where SVD decomposes a matrix into three sub-matrices in such a way that singular values get separated in the form of diagonal matrix [9]. The three decomposed matrices are: left singular matrix *U*, singular matrix *S*, and right singular matrix *V*, where *U* and *V* are the unitary matrices, and *S* is a diagonal matrix. Also, hidden information can be stored into specific LSB positions depending on the secret key. A sparse matrix generated by a private-key to determine the location of non-ROI modification, enhance the security of patient data [17-18].

In this paper a multiple medical image watermarking scheme based on DWT and SVD is implemented for robust watermark, and LSB based fragile watermarking technique for tamper detection using BCH *(Bose-Chaudhuri-Hocquenghem)* coding for noise detection and correction to enhance protection. The implementation of the BCH requires choosing a polynomial called the generator that is known to the transmitter and the receiver [19]. The transmitter performs the encoding procedure on the message stream to generate a certain number of check bits called a checksum. This checksum is appended to the message being transmitted. The receiver performs the decoding procedure, to verify that the checksum is valid. A BCH code with symbols from Galois field *GF*(2) (with two elements 0 and 1), with length 31 of the code word (message + checksum), and 16 message length which represents the binary message are used.

III. EXPERIMENTAL ANALYSIS

A. *Implementation of the structured RONI based watermark*

In Fig.3 block diagram for implementation of the structured watermark is illustrated.

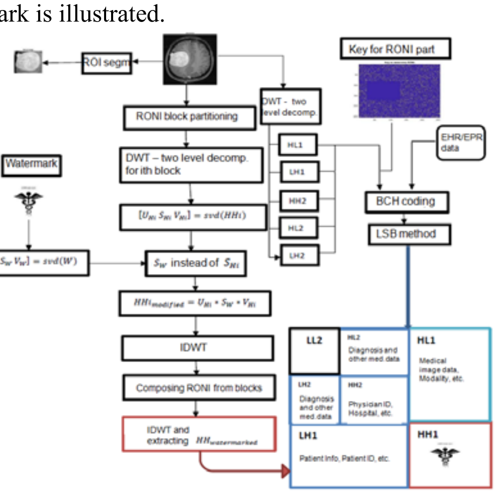

Fig. 3. Block diagram for implementation of the structured RONI and wavelet based watermark.

Robust watermark is implemented in transform domain, where 2-level DWT decomposition is applied, as well as SVD. ROI segmentation is performed, where its limits are memorized. This is followed by RONI partitioning to blocks of 8x8 pixels. For each block 2-level DWT is applied using Haar wavelet obtaining components noted as LL2, HL2, LH2, HH2, HL1, LH1 i HH1. Then, SVD is applied to HH1. SVD components of (logo) watermark are integrated to SVD components of the image. Finally, IDWT is applied for all the blocks of RONI part in order to compose the watermarked RONI. Watermarked HH1 part is related to robust approach.

For the fragile watermark, 2-level DWT is applied using Haar wavelet. Additional data is implemented in all parts except in the lowest and the highest frequencies (LL1, HH1). Textual data is divided into remaining bands, so that the diagnosis data belongs to HL2 and LH2, physician and hospital data belongs to HH2, patient info data belongs to LH1, and image data belongs to HL1 part. Private Key is generated in order not to affect the ROI while LSB method is applied for fragile watermark. This is a matrix of 256x256 pixels consisted of random numbers from 0 to 10, where zeros become 1, and the rest of the values become 0. Length of the message for watermarking is defined and the message itself is converted to binary representation. LSB method is applied along with BCH coding for textual data integration and for improved data security in order to keep data safe from unauthorized access. Coding word is of 31 bit length, while the message length is 16 bits, and the control sum is checked. If image pixel's LSB, where watermark is embedded equals to a corresponding bit of hidden message, the pixel remains the same. If this is not the case, bit corresponding to the message is put in that place. Finally, IDWT is applied on watermarked image so that fragile and robust parts can be composed into one final image.

B. *Digital watermark extraction*

Digital watermark extraction is illustrated in Fig.4.

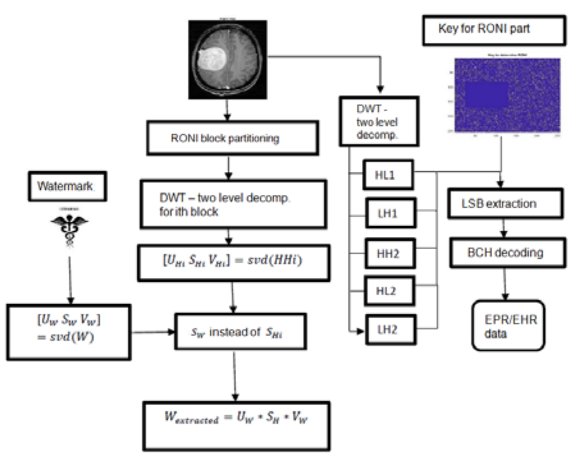

Fig. 4. Block diagram for digital watermark extraction.

Robust watermark is extracted similarly as in the implementation step. The ROI limits are used for obtaining RONI part of the watermarked image. This is followed by its partitioning, and applying 2-level DWT for obtaining the common ranges. The SVD approach is applied for HH1 part, and IDWT for logo watermark extraction. Similarly, as in the previous step with LSB extraction and BCH decoding fragile medical data can be extracted.

C. *Datasets and experimental phases*

Two sets are tested. The examples from the first set are presented in Fig.5 (PNG1-5), where the CT scans from [20] represent 24bit Covid-19 images in png format. Also, cancer CT [21], which are 16bit of the same resolution and in DICOM format, are investigated. They are illustrated in Fig.6 (DIC1-5). Here, only rectangle shape is assumed for ROI. ROI is selected manually, and is not part of this research. Thus, the method can be considered semi-automatic.

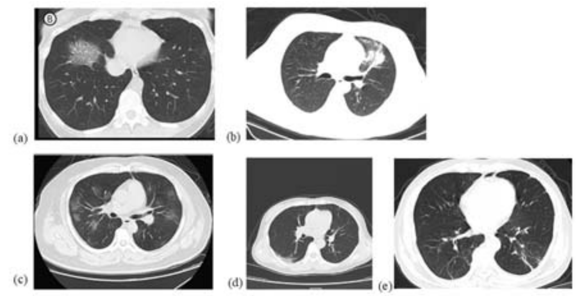

Fig. 5. Covid-19 CT chest scans: (a) 406x302 image, (b) 320x430 image, (c) 406x304 image, (d) 501x374 image, (e) 589x448 image, example.

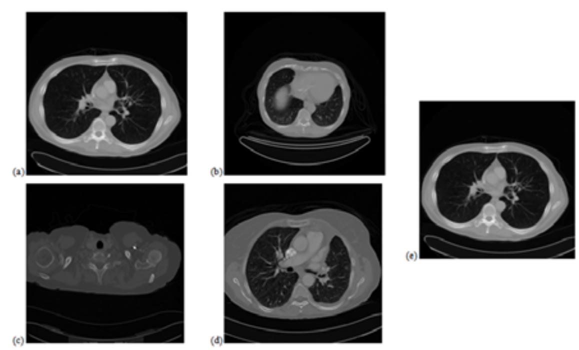

Fig. 6. Cancer CT 512x512 scans: (a)-(d) representing five DICOM images.

After the structured watermark integration and extraction model implementation, two logo watermarks (128x128) from Fig.2(a)-(b), and appropriate medical textual data as in Fig.2(c) are tested having in mind JPEG attack, as a common attack in image forensics. In the first phase of experimental analysis, the Covid-19 scans are tested, where PSNR (Peak-to-Signal Noise Ratio) and SSIM (Structural Similarity Index Metric) are calculated:

$$PSNR_{db}\left(I_{ref}, I_{tst}\right) = 10\log_{10}\frac{MAX_I^2}{MSE}, \quad (1)$$

$$MSE = \frac{1}{NxM}\sum_{i=0}^{N-1}\sum_{j=0}^{M-1}\left(I_{ref}(i,j) - I_{tst}(i,j)\right)^2, \quad (2)$$

$$SSIM\left(I_{ref}, I_{tst}\right) = L(I_{ref}, I_{tst})C(I_{ref}, I_{tst})S(I_{ref}, I_{tst}) \quad (3)$$

where in (1) MAX_I represents maximum intensity value and MSE is explained in (2). In (3) three factors representing luminance, contrast, and structure (L, C, S, respectively) are used for comparing reference and tested image (I_{ref}, I_{tst}). The second phase is similar, and PSNR and SSIM are calculated for the cancer CT dicom images, having in mind JPEG attack. Four different quality JPEG levels are tested (Q = 15, 30, 75, 100). In the third phase a comparison to [22] is performed.

IV. Experimental results

A. Experimental results for Covid-19 CT data under JPEG attacks

The obtained PSNR and SSIM results for Logo1 and Logo2, are shown in Fig.7(a) and Fig.7(b), respectively. The results are obtained for four JPEG quality (Q) levels, and five images PNG1-5. Extracted watermark Logo1 is shown in Fig.8. Similarly, the extraction results for Logo2 are shown in Fig.9.

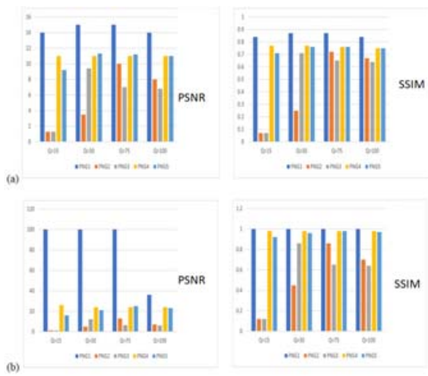

Fig. 7. PSNR and SSIM results under JPEG attacks for Covid-19 CT scans, and: (a) Logo1 and (b) Logo2.

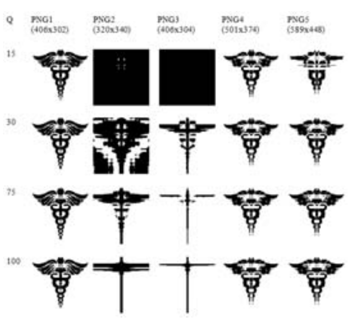

Fig. 8. Logo1 extraction results for Covid-19 scans under JPEG attacks.

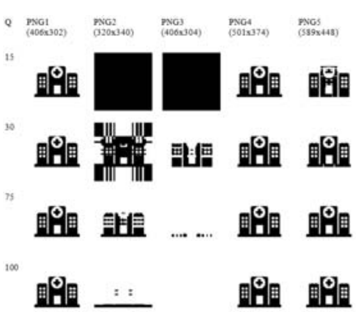

Fig. 9. Logo2 extraction results for Covid-19 scans under JPEG attacks.

B. Experimental results for Cancer CT data under JPEG attacks

The obtained PSNR and SSIM results for Logo1 and Logo2, are shown in Fig.10(a) and Fig.10(b), respectively. Extracted logos example is presented in Fig.11.

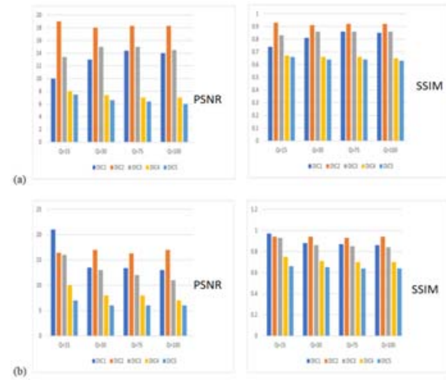

Fig. 10. PSNR and SSIM results under JPEG attacks for cancer CT scans, and: (a) Logo1 and (b) Logo2.

Fig. 11. Extracted (a) Logo1 and (b) Logo2 for DIC1 image and Q=30 quality.

C. Comparison results

The comparison is performed with another structured approach from literature [22]. The comparison results for PNG1-5 are presented in Fig.12. Similarly, the results for DICOM images are given in Fig.13, where Q1 denotes the quality for the method from [22].

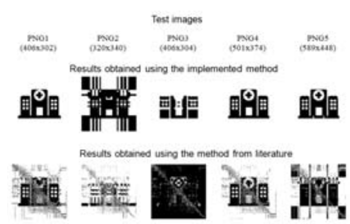

Fig. 12. Comparison results between the implemented method and the method from literature [22] for PNG images.

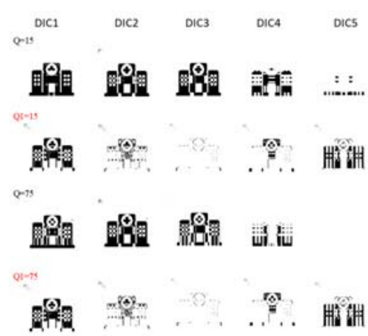

Fig. 13. Comparison results between the implemented method and the method from [22] for DICOM images.

PSNR and SSIM comparison results are illustrated in Fig.14 and Fig.15 for the first and the second dataset, respectively. The proposed method is compared to [22] which is based on DWT, Hessenberg decomposition and SVD.

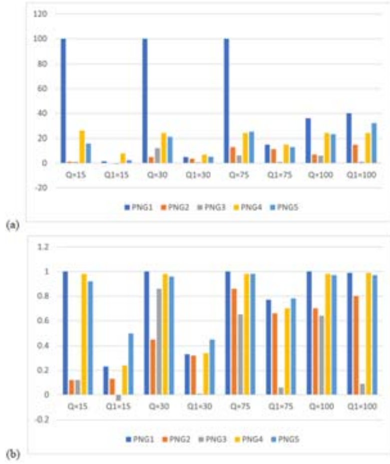

Fig. 14. (a) PSNR and (b) SSIM comparison results between the implemented method (Q) and the method [22] (Q1) for PNG images.

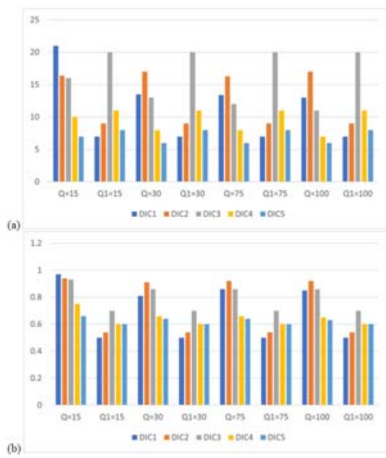

Fig. 15. (a) PSNR and (b) SSIM comparison results between the implemented method (Q) and the method [22] (Q1) for DICOM images.

In JPEG compression and similar tested attacks (except Gaussian filtering) fragile watermark is not extracted as original, which confirms that the manipulation occurred. Example of the extracted fragile watermark is shown in Fig.16.

Fig. 16 Example of unapropriatelly fragile watermark extraction.

JPEG compression could be recommended in certain cases, especially when medical or professional staff communicates via modern mobile applications that do not include support for the DICOM format (DICOM viewer). This should be done only for the purpose of more efficient informal communication.

In the current situation of the corona virus COVID-19, remote consultations were proposed to avoid cross-infection and regional differences in medical resources. However, the safety of digital medical imaging in remote consultations has also attracted more attention from the medical industry.

Covid-19 cases are often of different resolutions because of the use of different equipment and because of more efficient analyzes. With such data, ROI often has large dimensions, so it often occupies a larger part of the original image, which reduces the watermarking capacity. The influence of capacity on the robustness and perceptibility of watermarked image is not negligible. By increasing the data payload, the robustness will decrease and the perceptibility will increase. Dimensions (resolution) of the host image should also be further considered.

Image adjustment of size 512x512 pixels was applied before embedding the watermark. The worst results were obtained for PNG2 and PNG3, as shown for the extraction of both visual robust watermarks in Fig. 8-9. The PNG2 example has a lower resolution compared to the predefined image dimension adjustment, while the reason for PNG3 example was the image content itself, because similar image dimensions are in the PNG1 example. A similar experiment was done for dicom files, which correspond to cancer diagnostics. The obtained results are satisfactory because in most cases the watermark proved to be robust, i.e. it can be recognized. Text data during this attack in all formats could not be detected, which was the intention. The visual quality changes of selected medical images after watermark embedding are not noticeable, while the general image quality after watermark extraction is directly correlated with the extracted watermark quality discussed in this paper. Nevertheless, the RONI approach is recommended in order to prevent possible ROI changes.

The main contribution of this paper is the implementation of the DWT and RONI based watermarking for Covid-19 and other CT scans using robust and fragile approach, where the results showed the need for systematic approach for authentication in the case of available scans during pandemics, particularly having in mind JPEG attacks. The future experiments need to be performed for larger CT databases since other issues may occur besides lossy compression (e.g. due to segmentation).

V. CONCLUSION

This paper presents multiple/structured watermarking method which is based on RONI, as well a DWT, SVD, LSB and BCH techniques. Both robust and fragile watermarks are implemented. Analysis under JPEG compression attack showed watermark characteristics that can be useful for CT, like Covid-19 scans of different resolutions. Experimental results show that the model gives a good compromise between imperceptibility, robustness and fragility.

Future research should be directed towards enabling automatic CT scan watermarking, and further testing with larger database and watermarking method capacity.

ACKNOWLEDGMENT

This work was partially supported by the Ministry of Education, Science and Technological Development of the Republic of Serbia.

REFERENCES

[1] A. Anand and A. K. Singh, "Watermarking techniques for medical data authentication: a survey," *Multimedia Tools and Applications* pp. 1-33, 2020. https://doi.org/10.1007/s11042-020-08801-0.

[2] D. Laishram, and K. M. Singh, "A watermarking scheme for source authentication, ownership identification, tamper detection and restoration for color medical images," *Multimedia Tools and Applications*, pp. 1-61, 2021. https://doi.org/10.1007/s11042-020-10389-4

[3] X. Zhou, Y. Ma, Q. Zhang, M. A. Mohammed, and R. Damaševičius. "A Reversible Watermarking System for Medical Color Images: Balancing Capacity, Imperceptibility, and Robustness," *Electronics* 10, no. 9, pp. 1024, 2021.

[4] PACS sistemi, http://www.telemed.rs/pacs-sistemi/ (last accessed 03.05.2021.)

[5] A. Shehab, M. Elhoseny, K. Muhammad, A. K. Sangaiah, P. Yang, H. Huang, and G. Hou, "Secure and robust fragile watermarking scheme for medical images," *IEEE Access*, *6*, pp. 10269-10278, 2018.

[6] L. O. M. Kobayashi, S. S. Furuie, P. S. L.M. Barreto, "Providing integrity and authenticity in DICOM images: a novel approach," *IEEE Transactions on Information Technology in Biomedicine*, vol. 13, no. 4, pp. 582-589, 2009.

[7] V. Diaz-Flores-Garcia, et al., "Detecting the manipulation of digital clinical records in dental practice," *Radiography*, 23.4, pp.e103-e107, 2017.

[8] G. Coatrieux, H. Maitre, B. Sankur, "Strict integrity control of biomedical images," In *Security and watermarking of multimedia contents III,* International Society for Optics and Photonics, pp. 229-240, 2001.

[9] S. Mehta, et al., "A study of DWT and SVD based watermarking algorithms for patient privacy in medical images," In *2013 IEEE International Conference on Healthcare Informatics*, IEEE, pp. 287-296. 2013.

[10] K. A. Navas, et al., "Dwt-dct-svd based watermarking," In 3rd Int. Conference on Communication Systems Software and Middleware and Workshops (COMSWARE'08), IEEE, pp. 271-274, 2008.

[11] S.C. Liew, S.W. Liew, and J.M. Zain, "Reversible medical image watermarking for tamper detection and recovery with Run Length Encoding compression," *World Academy of Science, Engineering and Technology*, 72, pp. 799-803, 2010.

[12] T. BW Agung, et al., "Medical image watermarking with tamper detection and recovery using reversible watermarking with LSB modification and run length encoding (RLE) compression," In *2012 IEEE International Conference on Communication, Networks and Satellite (ComNetSat)*, IEEE, pp. 167-171, 2012.

[13] M. S. Nambakhsh, A. Ahmadian, and H. Zaidi, "A contextual based double watermarking of PET images by patient ID and ECG signal," *Computer methods and programs in biomedicine*, 104.3, pp. 418-425, 2011.

[14] A. Castiglione, et al., "On the protection of fMRI images in multi-domain environments," In: *2015 IEEE 29th International Conference on Advanced Information Networking and Applications*, IEEE, pp. 476-481, 2015.

[15] A. Giakoumaki, S. Pavlopoulos, D. Koutsouris, "Multiple image watermarking applied to health information management," *IEEE Transactions on Information Technology in Biomedicine*, 10.4, pp. 722-732, 2006.

[16] O. S. Pianykh, *Digital imaging and communications in medicine (DICOM): a practical introduction and survival guide*, Vol. 6, Berlin: Springer, 2008.

[17] Github, https://github.com/Sherry-SR/Wavelets_Watermarking (last accessed 01.04.2021.)

[18] Github, https://github.com/ArkaPM/Region-of-Interest-Based-Medical-Image-Compression (last accessed 01.04.2021.)

[19] Y. S. Han, *BCH codes*, Graduate Institute of Communication Engineering, National Taipei University Taiwan, 2010. http://ct.ee.ntust.edu.tw/BCH_code.pdf (last accessed 04.05.2021.)

[20] CT Covid data, https://github.com/UCSD-AI4H/COVID-CT/blob/master/Images-processed/CT_COVID.zip (last accessed 31.5.2021.)

[21] CT Medical Images, https://www.kaggle.com/kmader/siim-medical-images?select=dicom_dir (last accessed 31.5.2021.)

[22] Github, https://github.com/Saeid-jhn/Digital-Image-Watermarking (last accessed 01.06.2021.)